NANOSYSTEMS:
PHYSICS, CHEMISTRY, MATHEMATICS

Original article

Kharina S.N., et al. *Nanosystems: Phys. Chem. Math.*, 2024, **15** (3), 388–397.
http://nanojournal.ifmo.ru
DOI 10.17586/2220-8054-2024-15-3-388-397

Copper-modified g-C_3N_4/TiO_2 nanostructured photocatalysts for H_2 evolution from glucose aqueous solution

Sofiya N. Kharina[a], Anna Yu. Kurenkova[b], Andrey A. Saraev[c], Evgeny Yu. Gerasimov[d], Ekaterina A. Kozlova[e]

Boreskov Institute of Catalysis SB RAS, Novosibirsk, Russia

[a]skharina@catalysis.ru, [b]kurenkova@catalysis.ru, [c]asaraev@catalysis.ru, [d]gerasimov@catalysis.ru, [e]kozlova@catalysis.ru

Corresponding author: Sofiya N. Kharina, skharina@catalysis.ru

ABSTRACT Two strategies for synthesis of copper-modified composite photocatalysts based on graphitic carbon nitride and titanium dioxide for hydrogen evolution reaction are presented. The first one is based on the mechanical dispersion of separately prepared g-C_3N_4 and commercial TiO_2 (Evonik P25), modified with copper. Another approach is co-calcination of melamine and commercial TiO_2 with subsequent modification by copper. The samples were characterized using X-ray diffraction (XRD), UV-vis diffuse reflectance spectroscopy (UV-vis DRS), X-ray photoelectron spectroscopy (XPS), and high-resolution transmission electron microscopy (HRTEM). The synthesized photocatalysts were tested in hydrogen evolution from glucose aqueous solution under visible light irradiation (440 nm). The largest photocatalytic activities met 235 and 259 μmol·g^{-1}·h^{-1}, corresponding to the first and the second photocatalyst series, respectively. The most active photocatalyst from the first series 1 wt.% g-C_3N_4/1 wt.% CuO_n/TiO_2 maintained its hydrogen production rate during a 6-hour cyclic stability test.

KEYWORDS photocatalysis, photocatalytic H_2 production, biomass photoreforming, glucose photoconversion, composite photocatalysts, titanium dioxide, graphitic carbon nitride, visible light irradiation

ACKNOWLEDGEMENTS This study was supported by Russian Science Foundation, project No. 23-73-01161. Authors thank to A. V. Zhurenok for UV-Vis spectra measurements and D. D. Mishchenko for XRD analysis.

FOR CITATION Kharina S.N., Kurenkova A.Yu., Saraev A.A., Gerasimov E.Yu., Kozlova E.A. Copper-modified g-C_3N_4/TiO_2 nanostructured photocatalysts for H_2 evolution from glucose aqueous solution. *Nanosystems: Phys. Chem. Math.*, 2024, **15** (3), 388–397.

1. Introduction

To overcome the energy shortage and ensure the sustainable development of mankind, the use of hydrogen as an energy carrier rather than traditional fuels is considered to be the most reasonable trend. Despite the fact that hydrogen is mainly produced from non-renewable sources such as coal and natural gas, more attention must be paid to the use of renewable energy sources. The promising approach is the photoreforming of biomass. Its key advantages are simplicity, low operating cost, non-requirement of high pressure and temperature during the treatment and wide variety of catalysts [1, 2]. Moreover, this technique is not only based on solar energy inputs and inexhaustible biomass substrates, but could use the byproducts from industrial biomass conversion, e.g. alcohols (methanol, ethanol, glycerol, isopropanol), carboxylic acids (lactic, formic, acetic) mono-, di- and polysaccharides [3–11]. Although biomass-derived products have long been utilized as an energy source, they are often used for hydrogen production through high-energy consuming thermochemical or low-efficiency biorefinery processes. Therefore, developing an effective photoreforming process does remain of the great demand.

Titanium dioxide being one of the best n-type semiconducting and widely studied photocatalysts has been employed for various applications [12–14]. Providing its strong oxidizing and moderate reducing abilities, the band structure of TiO_2 limits its activity within the UV range. To shift its light absorption edge to a greater wavelength region, the use is made of visible light sensitive semiconductors. This helpful strategy is to obtain the heterostructure, which contains TiO_2 and some narrow-band gap semiconducting material intimately connected. The formation of heterojunction between two semiconductors leads to increased charge separation and, therefore, to higher light absorption efficiency [15–17].

Among the vary of prospective narrow band semiconductors [18, 19], graphitic carbon nitride g-C_3N_4 is believed to be a promising candidate. Its narrow band gap (2.7 eV) and the strongly negative conduction band position (-1.3 eV vs. NHE) make g-C_3N_4 an effective material for proton reduction with hydrogen formation under visible light [20–22]. In comparison with traditional photocatalysts being active under visible radiation – metal chalcogenides, the important advantages of g-C_3N_4 are non-toxicity and outstanding chemical and thermal stability (up to 600 °C) [23]. As many other

pristine semiconductors g-C_3N_4 suffers from the fast charge-carrier recombination, which restrains its application. To increase the life time of photogenerated charge carriers, a lot of efforts has been made to synthesize the composites based on g-C_3N_4 and wide bandgap semiconductors such as TiO_2. Such strategy allows one to promote the charge separation and increase their lifetime.

There are multiple photocatalytic applications where g-C_3N_4/TiO_2 is utilized [24], with H_2 production being among them. For instance, Hongjian [16] fabricated g-C_3N_4/TiO_2 by ball-milling, after than 0.5 wt.% Pt cocatalyst was photodeposited on the composite. The photocatalyst 50 % g-C_3N_4/TiO_2 has demonstrated the greatest H_2 production rate (22.4 mol·h^{-1}), which is twice as higher as unmodified g-C_3N_4. Another effective technique to modify semiconductor photocatalyst and increase the life time of photogenerated electrons and holes is the deposition of metal particles, such as Pt, Ni, Cu, etc., which act as electron mediators between two semiconductors. Bo Chai and colleagues [15] have developed g-C_3N_4/Pt/TiO_2 nanocomposite via a facile chemical adsorption followed by a calcination process. As a sacrificial agent the use was made of triethanolamine (TEOA) – one of the most effective electron donors for g-C_3N_4-based photocatalysts. The results have revealed the H_2 production rate rising with the increasing of g-C_3N_4 content and the activity reaching the maximum – 178 μmol·h^{-1} for the photocatalyst, which contains 30 % g-C_3N_4 loaded on Pt/TiO_2. A comprehensive study [17] has been carried out on ternary CdS/TiO_2/g-C_3N_4 composites applied both in H_2 evolution and dye degradation processes. The authors have reported that the system accomplishes an S-scheme heterojunction, which leads to enhanced photocatalyst activity compared to the individual components.

Despite the examples mentioned above, there is still insufficient information on studies that aim to expand the application area of g-C_3N_4 and its activation for photocatalytic H_2 production from biomass components. The article presented compares two different synthetic approaches for composite photocatalysts based on g-C_3N_4 and TiO_2 for H_2 generation from glucose aqueous solutions under visible light irradiation (440 nm). The main purpose of this work is to determine the effect of g-C_3N_4 loading on the photocatalytic activity of TiO_2 under visible light. Additionally, two synthetic strategies are proposed and their comparison is discussed herein. In our previous study [25] the influence of copper cocatalyst particles dispersed on TiO_2 was comprehensively discussed and it was found that CuO_n ($n = 0.5 - 1$) enhanced the photocatalytic H_2 evolution rate over TiO_2-based photocatalysts. In the present work, the CuO_n cocatalyst was used as well. Two series of nanostructured composites have been synthesized. The first one has been made through the mechanical dispersion of g-C_3N_4 and copper-modified TiO_2. To compare, the second series has been obtained by calcining melamine and TiO_2 mechanical mixture followed by copper deposition.

2. Experimental section

2.1. Photocatalyst characterization

The photocatalysts were analyzed by X-ray diffraction (XRD), UV-vis spectroscopy, X-ray photoelectron spectroscopy (XPS), and high-resolution transmission electron microscopy (HRTEM).

XRD pattern of the g-C_3N_4 was obtained using a D8 ADVANCE diffractometer equipped with a LYNXEYE linear detector (Bruker AXS GmbH, Karlsruhe, Germany) at room temperature in the 2θ of 10 – 60° with a step of 0.05° with Ni-filtered CuKα radiation ($\lambda = 1.5418$ Å). Diffuse reflectance UV-vis spectra were recorded using a UV-2501 PC spectrophotometer with an ISR-240A diffuse reflectance unit (Shimadzu, Kyoto, Japan). The morphology of the photocatalysts was studied by HRTEM using a ThemisZ electron microscope (Thermo Fisher Scientific, Waltham, MA, USA) at an accelerating voltage of 200 kV. The study of the chemical composition of the photocatalysts was carried out by XPS on an electronic spectrometer SPECS SurfaceNanoAnalysis GmbH (Germany). The spectrometer was equipped with a PHOIBOS-150-MCD-9 hemispherical analyzer, an XR-50 characteristic X-ray source with a double Al/Mg anode. Non-monochromatic MgKα radiation ($h\nu = 1253.6$ eV) was used to record the spectra. To take into account the effect of charging the samples, we used the position of the peak corresponding to titanium dioxide ($E(\mathrm{Ti2p_{3/2}}) = 458.7$ eV).

2.2. Synthesis of the photocatalysts

In order to synthesize the photocatalysts, all chemicals were taken in analytical grade without any additional purification.

2.2.1. TiO_2 pretreatment. TiO_2 samples were obtained using commercially available Evonik P25. Evonik P25 (0.500 g) was placed in a crucible and calcined at 600 – 750 °C for 3 h at a heating rate of 3 °C·min^{-1}. The resulting powder was then collected and ground thoroughly in a ceramic mortar.

2.2.2. g-C_3N_4 synthesis. Melamine was used as a precursor for graphitic carbon nitride formation via thermal condensation process. 20 g of melamine to be loaded in a covered crucible was heated to 600 °C at a rate of 10 °C·min^{-1} and held for 2 h. The yellow powder was ground in mortar for the further usage.

2.2.3. 1st series of composite photocatalysts. The first series of photocatalysts were obtained by copper deposition on the TiO_2 surface and subsequent dispersing it with g-C_3N_4. Copper loading (1 and 5 wt.%) was carried out via chemical precipitation route. A 0.1 M $Cu(NO_3)_2$ aqueous solution was added to proper amounts (495 and 475 g) of calcined or pristine TiO_2 and stirred for 1 hour. An excess of $NaBH_4$ aqueous solution was appended and the mixture was stirred for 1.5 hours followed by washing with deionized water and centrifugation. The damp precipitate was then dried at 60 °C in air during 12 hours. The samples containing 1 wt.% of CuO_n ($n = 0.5 - 1$) and TiO_2 calcined at different temperatures were separated off to investigate their photocatalytic properties. Further, 1 and 5 wt.% of g-C_3N_4 was mixed with 1 or 5 wt. % CuO_n/TiO_2-750 in acetone and kept under constant stirring at 50 °C for 60 minutes to obtain particles distributed homogeneously. Then the suspension was heated on a water bath until acetone evaporated and dried at 60 °C in air for 12 hours. The first series of composites was referred to as X-CN/Y-Cu/TiO_2-750 (where X and Y represent weight content of g-C_3N_4 and CuO_n respectively).

2.2.4. 2st series of composite photocatalysts. To obtain the second photocatalyst series, melamine and TiO_2-750 were mixed and ground in a mortar with mass ratios (wt. %) melamine : TiO_2 ranging from 10 : 90 to 50 : 50. The mixture was calcined under the same thermal treatment conditions as described above. Following the calcination, 1 wt. % of copper was deposited on the composite surface using the method mentioned in the previous paragraph. The composites were labelled as 1-Cu/X-M/TiO_2-750, where X represents the weight percentage of melamine.

2.3. Photocatalytic experiments

The photocatalytic activity tests were carried out in a glass reactor containing the quartz window and the sampler to analyze the gas phase (Fig. 1). The reaction mixture was obtained by suspending 50 mg of the photocatalyst in 100 ml 0.1 M glucose aqueous solution. Prior to each experiment, the reactor was purged with argon for 20 minutes to remove oxygen in the gas phase. The use was made of the commercially available visible light LED (440 nm, 580 mW·cm^{-2}) placed on a distance of 1 cm away from the quartz window. Also, the rate of H_2 evolution on the most active photocatalyst was studied under AM1.5G illumination using a sunlight simulator "Pico" (G2V Optics, Canada). Gas phase analysis was carried out using a gas chromatograph CHROMOS GC-1000 equipped with a thermal conductivity detector and a NaX zeolite column to determine the amount of H_2 evolved quantitatively.

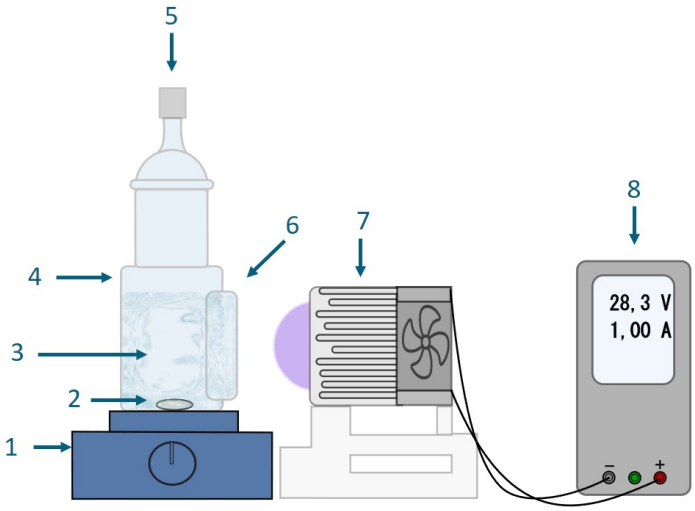

FIG. 1. Scheme of set-up for photocatalytic activity test. 1 – magnetic stirrer, 2 – stir bar, 3 – reaction suspension, 4 – glass reactor, 5 – sampler, 6 – quartz window, 7 – LED, 8 – power supply.

3. Results and discussions

3.1. Catalysts characterization

The photocatalyst synthesized were characterized by X-ray diffraction (XRD), diffuse reflectance spectroscopy (DRS), X-ray photoelectron spectroscopy (XPS), high-resolution transmission electron microscopy (HR TEM) and high-angle annular dark-field scanning transmission electron microscopy (HAADF-STEM).

The X-ray diffraction pattern of the synthesized g-C_3N_4 shown in Fig. 2a demonstrates two characteristic peaks at $2\theta = 12.8^\circ$ and 27.8°, which corresponds to the (210) and (002) crystal planes, respectively. The signal attributed to periodic stacking of triazine units is indicated as (210), thus suggesting that g-C_3N_4 forms a rhombic structure rather than a hexagonal structure.

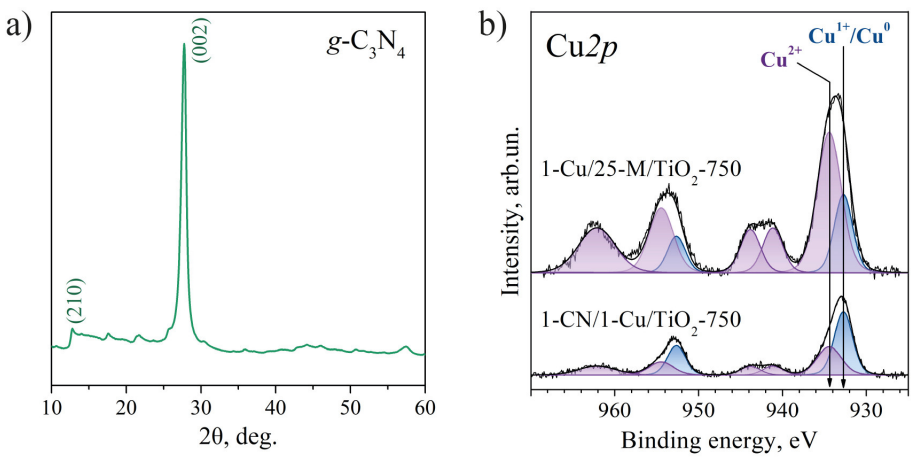

FIG. 2. a) XRD patterns of g-C_3N_4; b) Cu2p core-level spectra of photocatalysts. The spectra are normalized to the integral intensity of the corresponding Ti2p spectra.

The state and relative concentrations of elements in the surface layer of photocatalysts were analyzed by XPS (Table 1). At the survey spectra of the catalysts, peaks corresponding to Cu, Ti, N, C and O were found. The peaks related to g-C_3N_4 cannot be identified in the spectrum of C*1s* carbon due to the low concentration of g-C_3N_4 in the photocatalysts studied and the presence of carbon impurities from the atmosphere. The g-C_3N_4 content was estimated based on analysis of the N*1s* spectrum. It is worth noting that the near-surface layer of the photocatalyst 1-CN/1-Cu/TiO_2-750 contains a larger amount of nitrogen compared to the sample 1-Cu/25-M/TiO_2-750. At the same time, the concentration of copper on the surface, on the contrary, is higher in the case of 1-Cu/25-M/TiO_2-750. The g-C_3N_4 concentration in these photocatalysts may indeed differ due to different syntheses, however, since copper is deposited using the same method, its content in the volume of photocatalysts should be the same. It can be concluded that, in the case of the 1-CN/1-Cu/TiO_2-750 sample, the copper particles are partially shielded by g-C_3N_4; while in the 1-Cu/25-M/TiO_2-750 photocatalyst, copper is predominantly located on the surface of the photocatalyst.

TABLE 1. Relative atomic concentrations of elements in the surface area of the photocatalysts and N*1s*, Cu$2p_{3/2}$, and Ti$2p_{3/2}$ binding energies

Photocatalysts	**[N]/[Ti]**	**[Cu]/[Ti]**	**$Cu^{0/1+}$, %**	**N*1s***			**Cu$2p_{3/2}$**		**Ti$2p_{3/2}$**
				C–N=C	**$(C)_3$-N**	**N–H**	**$Cu^{0/1+}$**	**Cu^{2+}**	**TiO_2**
1-CN/1-Cu/TiO_2-750	0.11	0.07	50	398.7	400.0	401.1	932.7	934.5	458.7
1-Cu/25-M/TiO_2-750	0.04	0.22	20	398.7	400.0	401.1	932.7	934.5	458.7

The Cu*2p* spectra demonstrates the presence of copper in the Cu^{2+}, Cu^{+}, and/or Cu^0 states (Fig. 2b). The Cu*2p* core-level spectrum of both shows two intense Cu$2p_{3/2}$ and Cu$2p_{1/2}$ peaks at 932.7 and 952.7 eV and corresponding core-level satellite peaks at 941.1 – 943.8 eV and 962.1 eV, respectively. The presence of satellite peaks is observed for Cu^{2+} state, while Cu*2p* spectrum of $Cu^{0/1+}$ does not have the satellite peaks [26, 27]. The Cu$2p_{3/2}$ peak at 932.7 eV corresponds to copper in the metallic and/or Cu^{1+} state. Due to the close binding energies of the corresponding Cu$2p_{3/2}$ peaks, it is quite difficult to distinguish the Cu^0 and Cu^{1+} state by XPS technique [26, 28].

The UV-vis diffuse reflection spectra and Tauc plots of the photocatalysts are shown in Fig. 3. To plot the absorption spectra in Tauc coordinates the adsorption coefficient F(R) was found from the DRS data using the Kubelka–Munk equation [25] (1):

$$F(R) = \frac{(1-R)^2}{2R}, \tag{1}$$

where R is the reflection coefficient of the sample. When comparing the spectra of 1 % CuO_n/TiO_2 and pure TiO_2 (Fig. 3a), it is evident that the absorption edge of 1 % CuO_n/TiO_2 has shifted to the long-wavelength region and the reflection decreases within the 500 – 800 nm. Such effect suggests that the separation of photogenerated electron-hole pairs in the CuO_n/TiO_2 heterojunction has been effectively improved [29–31]. Notably, there is almost no difference observed between 1-CN/1-Cu/TiO_2 and 1-Cu/25-M/TiO_2. The composites reflectance spectra are characterized by a

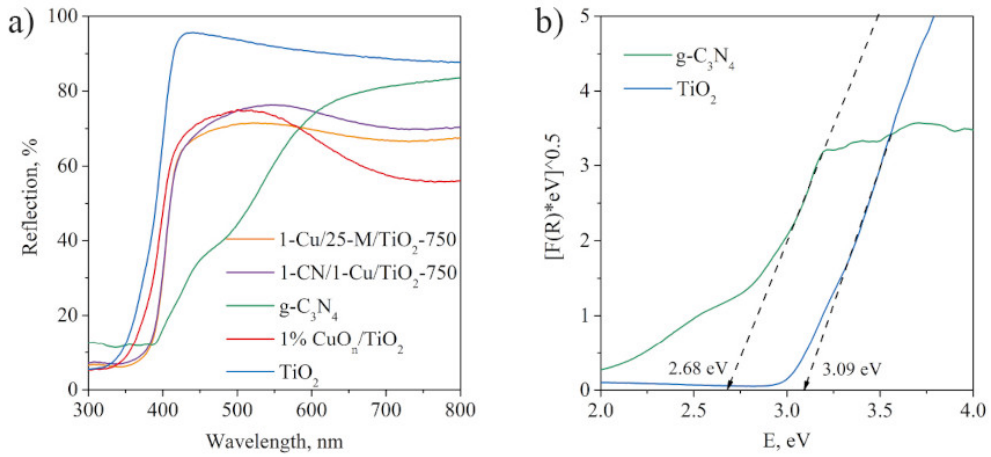

FIG. 3. (a) UV-VIS spectra for the TiO_2, g-C_3N_4, 1 % CuO_n/TiO_2, 1-CN/1-Cu/TiO_2-750 and 1-Cu/25-M/TiO_2-750 and (b) Tauc plots for the TiO_2 and g-C_3N_4

greater redshift compared with 1 % CuO_n/TiO_2. The results obtained consider, that modifying TiO_2 with a small amount (1 – 2 wt.%) of narrow band semiconductors enhances light harvesting and promotes photocatalytic activity under visible light irradiation.

The study of morphology of the 1-CN/1-Cu/TiO_2-750 photocatalyst showed that the composite consists of well-crystallized TiO_2 polyhedrons covered with copper nanoparticles and 2D nanosheets of g-C_3N_4 (Fig. 4a,b). Due to the fact that copper deposition has been followed by composite synthesis, g-C_3N_4 surface is copper-free. The size of TiO_2 particles is in the range of 20 – 200 nm, while copper particles have a narrow particle size distribution not exceeding the value of 5 nm (Fig. 4c). The photocatalyst microstructure was investigated in details using EDS elemental mapping. Despite the tendency of g-C_3N_4 layers to stick together, the EDS analysis (Fig. 4d,e,f) shows that the elements are uniformly distributed across the entire catalyst surface.

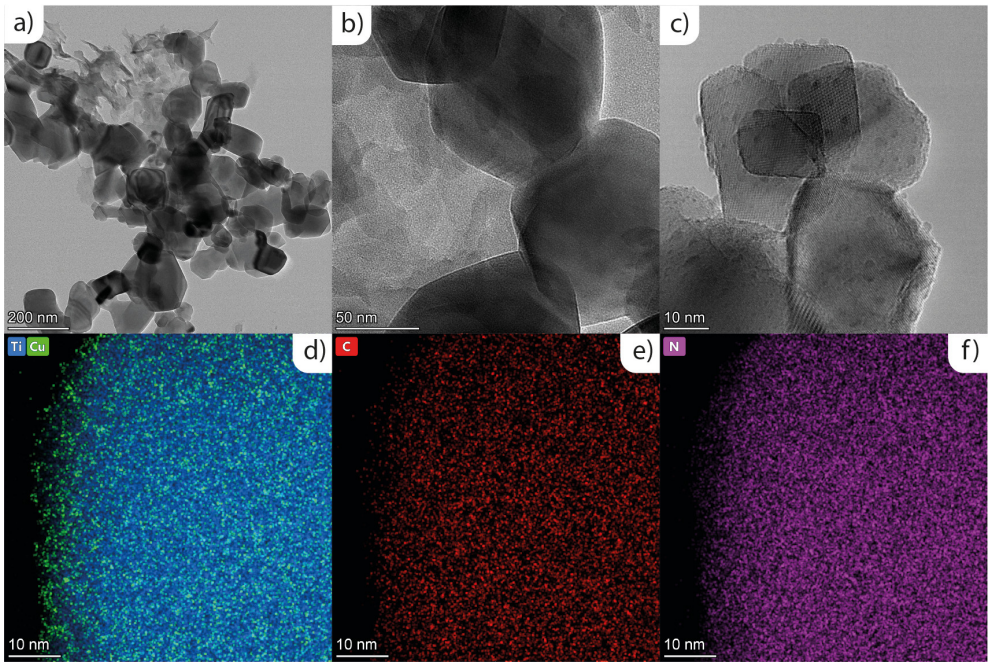

FIG. 4. TEM images and HAADF analysis with EDS of 1-CN/1-Cu/TiO_2-750

Although, different synthetic processes have been applied, the morphology of 1-Cu/10-M/TiO_2-750 (as shown in Fig. 5) resembles one for 1-CN/1-Cu/TiO_2-750. As the sample discussed previously, 1-Cu/25-M/TiO_2-750 has well-distinguished particles with an average diameter from 20 to 200 nm. The TEM image (Fig. 5c) displays some CuO_n nanoparticles (with average diameter of less than 5 nm) adsorbed onto the photocatalyst surface. Due to visually unresolved crystal structure in the Fig. 5c, the photocatalyst surface is believed to consist of TiO_2 in intimate contact with g-C_3N_4 and CuO_n hemispheres on top. Moreover, g-C_3N_4 is clearly seen to have extended nanosheet morphology as

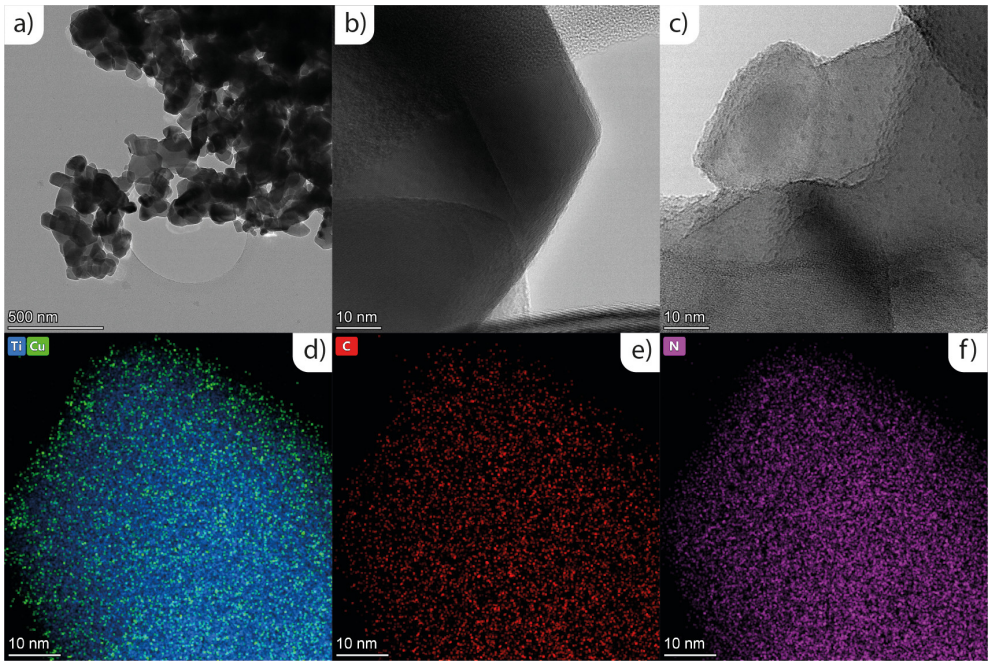

FIG. 5. TEM images and HAADF analysis with EDS of 1-Cu/25-M/TiO_2-750

presented in Fig. 5b. Finally, HAADF analysis with elemental mapping demonstrates uniformly distribution of CuO_n and g-C_3N_4 particles on the TiO_2 surface.

3.2. Photocatalytic activity

At the beginning, synergistic effect of TiO_2 modification with g-C_3N_4 and copper cocatalyst was investigated. The activities of unmodified TiO_2, 1 wt.% Cu/TiO_2, 1 wt.% g-C_3N_4/TiO_2, and 1 wt.% g-C_3N_4/1 wt.% Cu/TiO_2 photocatalysts were tested in the H_2 evolution reaction from glucose solution under visible light irradiation (440 nm). The deposition of g-C_3N_4 and copper leads to a decrease in the rate of H_2 evolution compared to unmodified TiO_2, probably due to a decrease in the adsorption of glucose on the surface of the photocatalyst (Fig. 6a). However, the co-deposition of both g-C_3N_4 and CuO_n on the TiO_2 surface promotes the rate of H_2 evolution. This synergistic effect is caused by an increase in light absorption by the composite photocatalyst and an increase in the lifetime of photogenerated charge carriers.

In the previous works, we studied the effect of calcination of TiO_2 on photocatalytic activity and showed that heat treatment in some cases leads to an increase in the activity of the photocatalyst [32]. Therefore, further for the synthesis of composite photocatalysts, TiO_2 was calcined at 750 °C.

The first series of photocatalysts was tested in the photocatalytic H_2 production from glucose aqueous solution. The results obtained are summarized in the Fig. 6b and Table 2. The maximum activity of 235 μmol·h^{-1}·g^{-1} is achieved for 1-CN/1-Cu/TiO_2-750, considering the variation of g-C_3N_4 content. Further increasing the g-C_3N_4 loading up to 5 wt.% causes a decline in activity to 174 μmol·h^{-1}·g^{-1}. Additionally, an increase in copper loading results in a decrease in the H_2 production rate, consistent with the earlier study [25]. However, the activity of all composite photocatalysts significantly exceeds the activity of commercial TiO_2.

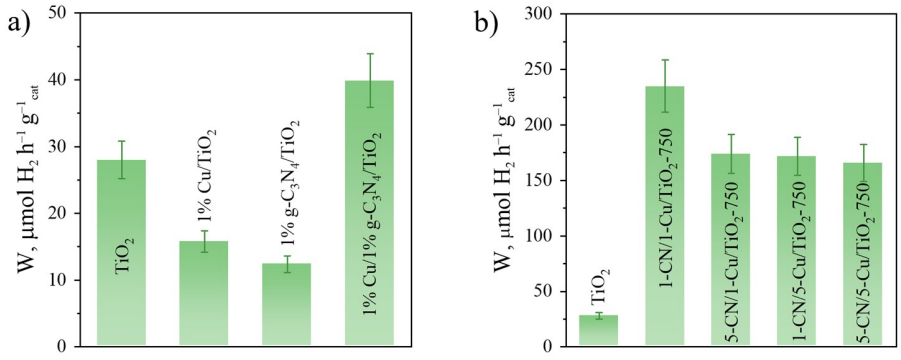

FIG. 6. Photocatalytic activity of the first photocatalyst series depending on copper and g-C_3N_4 amount

To investigate the impact of the synthetic method on photocatalyst activity, we examined the second series of composites under the same conditions (Fig. 7). Starting with the equal melamine: TiO_2 ratio, the H_2 production rate increases from 172 up to 259 μmol·h^{-1}·g^{-1} (Table 2) for 1-Cu/50-M/TiO_2 and 1-Cu/25-M/TiO_2, respectively. However, decreasing the melamine content may slightly depress the photocatalytic activity. The trend involved is observed for the previous photocatalyst as well. When g-C_3N_4 content raised, it covers the large portion of TiO_2 surface and impedes the glucose adsorption due to low affinity. The samples, corresponding to 10 and 25 wt.% melamine content before calcination, exhibit 243 and 259 μmol·h^{-1}·g^{-1}, respectively. These values are comparable to each other and indicate that the samples are among the most prominent photocatalysts in the series concerned.

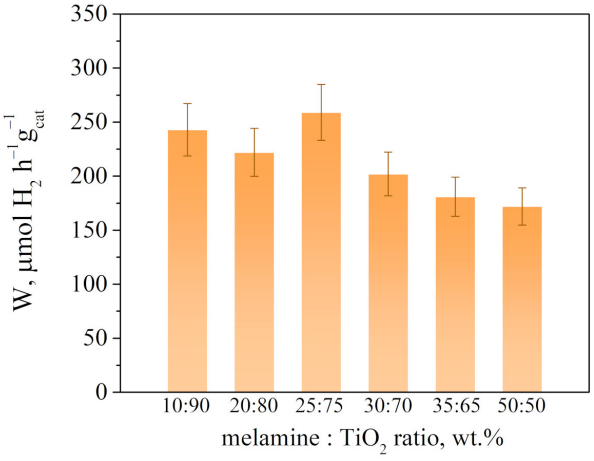

FIG. 7. Photocatalytic activity of the second photocatalyst series depending on melamine: TiO_2 mass ratio. Photocatalysts: 1-Cu/X-M/TiO_2-750.

The rate of H_2 evolution under the solar light was determined using the most active photocatalyst 1-Cu/25-M/TiO_2-750 (Table 3). Its activity is on par with other data in the literature and is inferior only to data obtained using a more powerful light source. In addition, it is worth noting that this photocatalyst does not contain expensive platinum group metals and can be synthesized from available precursors. The synthetic approach proposed in the work can significantly reduce the cost of the generated H_2 solar fuel.

3.3. Photocatalytic stability test

In our previous work, it has been established for CuO_n/TiO_2 photoactivity that it is fluctuant and dramatically decreases under long-term light irradiation [38]. To test the impact of g-C_3N_4 loading on the catalyst stability, we are to screen the 1-CN/1-Cu/TiO_2-750 in cyclic experiments. As shown in Fig. 8, the H_2 amount on 1-CN/1-Cu/TiO_2-750 does not lower significantly after each cycle and the rate of H_2 evolution is the same within the experimental error. It is worth mentioning that the addition of g-C_3N_4 allows increasing the stability of copper-modified TiO_2, if compare to the previous study. Thus, this fact suggests composite heterostructure with g-C_3N_4 being responsible for enhanced reusability of the catalyst.

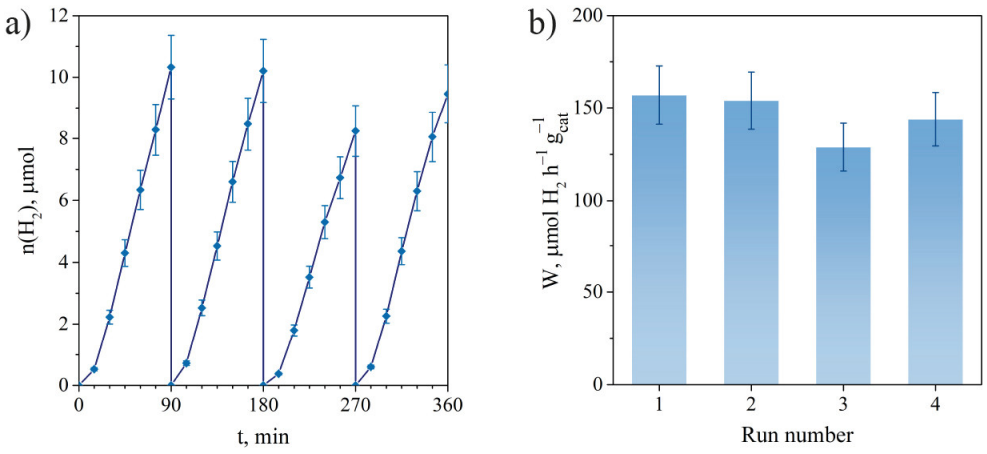

FIG. 8. Photocatalytic stability test: the kinetic curves of H_2 production (a), the dependence of H_2 generation rate on cycle number (b)

TABLE 2. Activities of the photocatalysts synthesized

Photocatalyst	**Designation**	**W(H_2), μmol·g^{-1}·h^{-1}**
TiO_2 unmodified		28
1st series of photocatalysts		
1 % g-C_3N_4 |1 % CuO_n |TiO_2-750	1-CN/1-Cu/TiO_2-750	235
5 % g-C_3N_4 |1 % CuO_n |TiO_2-750	5-CN/1-Cu/TiO_2-750	174
1 % g-C_3N_4 |5 % CuO_n |TiO_2-750	1-CN/5-Cu/TiO_2-750	172
5 % g-C_3N_4 |5 % CuO_n |TiO_2-750	5-CN/5-Cu/TiO_2-750	166
2st series of photocatalysts		
1 % CuO_n |g-C_3N_4 |TiO_2-750 (melamine : TiO_2 = 10 : 90)	1-Cu/10-M/TiO_2-750	243
1 % CuO_n |g-C_3N_4 |TiO_2-750 (melamine : TiO_2 = 20 : 80)	1-Cu/20-M/TiO_2-750	222
1 % CuO_n |g-C_3N_4 |TiO_2-750 (melamine : TiO_2 = 25 : 75)	1-Cu/25-M/TiO_2-750	259
1 % CuO_n |g-C_3N_4 |TiO_2-750 (melamine : TiO_2 = 30 : 70)	1-Cu/30-M/TiO_2-750	202
1 % CuO_n |g-C_3N_4 |TiO_2-750 (melamine : TiO_2 = 35 : 50)	1-Cu/35-M/TiO_2-750	181
1 % CuO_n |g-C_3N_4 |TiO_2-750 (melamine : TiO_2 = 50 : 50)	1-Cu/50-M/TiO_2-750	172

TABLE 3. The comparison of activity values of the photocatalysts based on g-C_3N_4 and TiO_2 with previously published data on H_2 photogeneration from a glucose solution

No.	**Photocatalyst**	**Conditions**			**W(H_2), μmol·g^{-1}·h^{-1}**	**Article**
		C_0(glucose)	**C(catalyst)**, g·L^{-1}	**Light source**		
1	1-Cu/25-M/TiO_2-750	0.1 M	0.5	Simulated solar light (AM1.5G, 100 mW/cm^2)	295	Present work
2	3 wt. % Pt/O-g-C_3N_4	0.1 M	0.25	Simulated solar light (500 W/m^2)	870	[33]
3	0.5 wt. % Pd/TiO_2	0.5 g·L^{-1}	0.5	LED, 375 – 380 nm, 1.5 W/m^2	590	[34]
4	2 wt. % PtAu/g- C_3N_4	0.16 M (pH = 13)	0.3	Xenon lamp (350 – 800 nm, 170 mW/cm^2)	2370	[35]
5	W- and N-doped Pt-TiO_2	1 mM	1.0	Natural solar irradiation	1000	[36]
6	$Cd_{0.8}Zn_{0.2}S$/Au/g-C_3N_4	0.1 M	0.5	Xenon lamp ($\lambda > 420$ nm)	123	[37]

4. Conclusion

This work proposed and investigated new photocatalysts based on TiO_2 and g-C_3N_4 for H_2 production from glucose aqueous solution under visible radiation (440 nm) and solar light (AM1.5G). Two series of photocatalysts were synthesized: one by mechanically dispersing g-C_3N_4 with TiO_2 and the other by co-calcinating melamine and TiO_2. The structure and properties of photocatalysts were established using the complex of physicochemical methods. The deposition of CuO_n and g-C_3N_4 particles on the TiO_2 surface was shown to alter its optical properties, resulting in a redshift of the absorption edge. Photocatalytic experiments were conducted to test the H_2 evolution rate over the samples obtained. The first series had a maximum rate of 235 μmol·h^{-1}·g^{-1}, while the second series – 259 μmol·h^{-1}·g^{-1} (440 nm), corresponding to 1-CN/1-Cu/TiO_2-750 and 1-Cu/25-M/TiO_2-750, respectively. The cyclic stability tests of the 1-CN/1-Cu/TiO_2-750 showed the rate of photocatalytic H_2 evolution kept the same during 4 cycle of experiments. Thus, in this work, active and stable photocatalysts were proposed for the production of H_2 under the solar light. It is worth noting that these photocatalysts could be obtained from inexpensive and available precursors such melamine, copper nitrate, and commercial TiO_2.

References

[1] Kou J., Lu, C., Wang J., Chen Y., Xu Z., Varma R.S. Selectivity Enhancement in Heterogeneous Photocatalytic Transformations. *Chem. Rev.*, 2017, **117** (3), P. 1445–1514.

[2] de Assis G.C., Silva I.M.A., dos Santos T.G., dos Santos T. V. Meneghetti M.R., Meneghetti S.M.P. Photocatalytic Processes for Biomass Conversion. *Catal. Sci. Technol.*, 2021, **11** (7), P. 2354–2360.

[3] Valeeva A.A., Dorosheva I.B., Kozlova E.A., Sushnikova A.A., Yu A., Saraev A.A., Schroettner H., Rempel A.A. Solar Photocatalysts Based on Titanium Dioxide Nanotubes for Hydrogen Evolution from Aqueous Solutions of Ethanol. *Int. J. Hydrogen Energy*, 2021, **46** (32), P. 16917–16924.

[4] Kurnosenko S.A., Zvereva I.A., Voytovich V. V., Silyukov O.I., Rodionov I.A. Photocatalytic Activity and Stability of Organically Modified Layered Perovskite-like Titanates $HLnTiO_4$ (Ln = La, Nd) in the Reaction of Hydrogen Evolution from Aqueous Methanol. *Catalysts*, 2023, **13** (4), 749.

[5] Kurnosenko S.A., Voytovich V.V., Silyukov O.I., Rodionov I.A., Zvereva I.A. Photocatalytic Hydrogen Production from Aqueous Solutions of Glucose and Xylose over Layered Perovskite-like Oxides $HCa_2Nb_3O_{10}$, $H_2La_2Ti_3O_{10}$ and Their Inorganic-Organic Derivatives. *Nanomaterials*, 2022, **12** (15), 2717.

[6] Samage A., Gupta P., Halakarni M.A., Nataraj S.K., Sinhamahapatra A. Progress in the Photoreforming of Carboxylic Acids for Hydrogen Production. *Photochem.*, 2022, **2** (3), P. 580–608.

[7] Imizcoz M., Puga A.V. Acid Photoreforming on Cu/TiO_2. *Catalysis Science & Technology*, 2019, **9** (5), P. 1098–1102.

[8] Davis K.A., Yoo S., Shuler E.W., Sherman B.D., Lee S., Leem G. Photocatalytic Hydrogen Evolution from Biomass Conversion. *Nano Convergence*, 2021, **8** (6), P. 1–19.

[9] Huang Z., Luo N., Zhang C., Wang F. Radical Generation and Fate Control for Photocatalytic Biomass Conversion. *Nature Reviews Chemistry*, 2022, **6**, P. 197–214.

[10] Butburee T., Chakthranont P., Phawa C., Faungnawakij K. Beyond Artificial Photosynthesis: Prospects on Photobiorefinery. *Chem. Cat. Chem.*, 2020, **12** (7), P. 1873–1890.

[11] Liu X., Duan X., Wei W., Wang S., Ni B.J. Photocatalytic Conversion of Lignocellulosic Biomass to Valuable Products. *Green Chemistry*, 2019, **21**, P. 4266–4289.

[12] Chu Y.M., Bach Q.V. Application of TiO_2 Nanoparticle for Solar Photocatalytic Oxidation System. *Appl. Nanosci.*, 2023, **13** (3), P. 1729–1736.

[13] Qian R., Zong H., Schneider J., Zhou G., Zhao T., Li Y., Yang J., Bahnemann D.W., Pan J.H. Charge Carrier Trapping, Recombination and Transfer during TiO_2 Photocatalysis: An Overview. *Catal. Today*, 2019, **335**, P. 78–90.

[14] Shiraishi Y., Hirai T. Selective Organic Transformations on Titanium Oxide-Based Photocatalysts. *J. of Photochemistry and Photobiology C: Photochemistry Reviews*, 2008, **9** (4), P. 157–170.

[15] Chai B., Peng T., Mao J., Li K., Zan L. Graphitic Carbon Nitride (g-C_3N_4)-Pt-TiO_2 Nanocomposite as an Efficient Photocatalyst for Hydrogen Production under Visible Light Irradiation. *Phys. Chem. Chem. Phys.*, 2012, **14** (48), P. 16745–16752.

[16] Yan H., Yang H. TiO_2-g-C_3N_4 Composite Materials for Photocatalytic H_2 Evolution under Visible Light Irradiation. *J. of Alloys and Compounds*, 2011, **509** (4), L26–L29.

[17] Shoaib M., Naz M.Y., Shukrullah S., Munir M.A., Irfan M., Rahman S., Ghanim A.A.J. Dual S-Scheme Heterojunction CdS/TiO_2/g-C_3N_4 Photocatalyst for Hydrogen Production and Dye Degradation Applications. *ACS Omega*, 2023, **8** (45), P. 43139–43150.

[18] Wei D.W., DuChene J.S., Sweeny B.C., Wang J., Niu W. Current Development of Photocatalysts for Solar Energy Conversion. *New and Future Developments in Catalysis: Solar Photocatalysis*, Elsevier, USA, 2013, P. 279–304.

[19] Li J., Chu D. Energy Band Engineering of Metal Oxide for Enhanced Visible Light Absorption. *Multifunctional Photocatalytic Materials for Energy*, 2018, P. 49–78.

[20] Ye S., Wang R., Wu M.Z., Yuan Y.P. A Review on g-C_3N_4 for Photocatalytic Water Splitting and CO_2 Reduction. *Applied Surface Science*, 2015, **358**, P. 15–27.

[21] Mamba G., Mishra A.K. Graphitic Carbon Nitride (g-C_3N_4) Nanocomposites: A New and Exciting Generation of Visible Light Driven Photocatalysts for Environmental Pollution Remediation. *Appl. Catal. B Environ.*, 2016, **198**, P. 347–377.

[22] Zheng Y., Lin L., Wang B., Wang, X. Graphitic Carbon Nitride Polymers toward Sustainable Photoredox Catalysis. *Angew. Chemie – Int. Ed.*, 2015, **54** (44), P. 12868–12884.

[23] Dong J., Zhang Y., Hussain M.I., Zhou W., Chen Y., Wang L.N. g-C_3N_4: Properties, Pore Modifications, and Photocatalytic Applications. *Nanomaterials*, 2021, **12** (1), 121.

[24] Lingzhiiwangg J.B., Juyingglei M. *Photocatalysis Fundamentals, Materials and Applications*, Springer, Singapore, 2018, 414 p.

[25] Kurenkova A.Y., Yakovleva A.Y., Saraev A.A., Gerasimov E.Y., Kozlova E.A., Kaichev V.V. Copper-Modified Titania-Based Photocatalysts for the Efficient Hydrogen Production under UV and Visible Light from Aqueous Solutions of Glycerol. *Nanomaterials*, 2022, **12** (18), 3106.

[26] Wöllner A., Lange F., Schmelz H., Knözinger H. Characterization of Mixed Copper-Manganese Oxides Supported on Titania Catalysts for Selective Oxidation of Ammonia. *Appl. Catal. A, Gen.*, 1993, **94** (2), P. 181–203.

[27] Fedorov A., Saraev A., Kremneva A., Selivanova A., Vorokhta M., Šmíd, B., Bulavchenko, O., Yakovlev, V., Kaichev, V. Kinetic and Mechanistic Study of CO Oxidation over Nanocomposite Cu–Fe–Al Oxide Catalysts. *Chem. Cat. Chem.*, 2020, **12** (19), P. 4911–4921.

[28] Bukhtiyarov V.I., Kaichev V.V., Prosvirin I.P. X-Ray Photoelectron Spectroscopy as a Tool for in-Situ Study of the Mechanisms of Heterogeneous Catalytic Reactions. *Top. Catal.*, 2005, **32** (1–2), P. 3–15.

[29] Muscetta M., Andreozzi R., Clarizia L., Di Somma I., Marotta R. Hydrogen Production through Photoreforming Processes over Cu_2O/TiO_2 Composite Materials: A Mini-Review. *Int. J. Hydrogen Energy*, 2020, **45** (53), P. 28531–28552.

[30] Nishikiori H., Harata N., Yamaguchi S., Ishikawa T., Kondo H., Kikuchi A., Yamakami T., Teshima K. Formation of CuO on TiO_2 Surface Using Its Photocatalytic Activity. *Catalysts*, 2019, **9** (4), 383.

[31] Segovia-Guzmán M.O., Román-Aguirre M., Verde-Gomez J.Y., Collins-Martínez V.H., Zaragoza-Galán G., Ramos-Sánchez V.H. Green Cu_2O/TiO_2 Heterojunction for Glycerol Photoreforming. *Catal. Today*, 2020, **349**, P. 88–97.

[32] Kurenkova A.Y., Kremneva A.M., Saraev A.A., Murzin V., Kozlova E.A., Kaichev V.V. Influence of Thermal Activation of Titania on Photoreactivity of Pt/TiO_2 in Hydrogen Production. *Catal. Letters*, 2021, **151**, P. 748–754.

[33] Speltini A., Scalabrini A., Maraschi F., Sturini M., Pisanu A., Malavasi L., Profumo A. Improved Photocatalytic H_2 Production Assisted by Aqueous Glucose Biomass by Oxidized g-C_3N_4. *Int. J. Hydrogen Energy*, 2018, **43** (32), P. 14925–14933.

[34] Vaiano V., Iervolino G., Sarno G., Sannino D., Rizzo L., Murcia Mesa J. J., Hidalgo M.C., Navío J.A. Production Simultanée de CH_4 et H_2 Par Réformage Photocatalytique d'une Solution Aqueuse de Glucose Sur Un Catalyseur Pd-TiO_2 Sulfaté. *Oil Gas Sci. Technol.*, 2015, **70** (5), P. 891–902.

[35] Ding F., Yu H., Liu W., Zeng X., Li S., Chen L., Li B., Guo J., Wu C. Au-Pt Heterostructure Cocatalysts on g-C_3N_4 for Enhanced H_2 Evolution from Photocatalytic Glucose Reforming. *Mater. Des.*, 2024, **238**, 112678.

[36] Bellardita M., García-López E. I., Marcì G., Nasillo G., Palmisano, L. Photocatalytic Solar Light H_2 Production by Aqueous Glucose Reforming. *Eur. J. Inorg. Chem.*, 2018, **41**, P. 4522–4532.

[37] Zhao H., Ding X., Zhang B., Li Y., Wang C. Enhanced Photocatalytic Hydrogen Evolution along with Byproducts Suppressing over Z-Scheme $Cd_xZn_{1-x}S$/Au/g-C_3N_4 Photocatalysts under Visible Light. *Sci. Bull.*, 2017, **62** (9), P. 602–609.

[38] Kozlova E.A., Kurenkova A.Y., Gerasimov E.Y., Gromov N.V., Medvedeva T.B., Saraev A.A., Kaichev V.V. Comparative Study of Photoreforming of Glycerol on Pt/TiO_2 and CuO_x/TiO_2 Photocatalysts under UV Light. *Mater. Lett.*, 2021, **283**, 128901.

Submitted 18 April 2024; revised 9 May 2024; accepted 10 May 2024

Information about the authors:

Sofiya N. Kharina – Boreskov Institute of Catalysis SB RAS, Lavrentieva Ave, 5, Novosibirsk, 630090, Russia; ORCID 0009-0000-9399-0231; skharina@catalysis.ru

Anna Yu. Kurenkova – Boreskov Institute of Catalysis SB RAS, Lavrentieva Ave, 5, Novosibirsk, 630090, Russia; ORCID 0000-0002-4150-7049; kurenkova@catalysis.ru

Andrey A. Saraev – Boreskov Institute of Catalysis SB RAS, Lavrentieva Ave, 5, Novosibirsk, 630090, Russia; ORCID 0000-0001-9610-9921; asaraev@catalysis.ru

Evgeny Yu. Gerasimov – Boreskov Institute of Catalysis SB RAS, Lavrentieva Ave, 5, Novosibirsk, 630090, Russia; ORCID 0000-0002-3230-3335; gerasimov@catalysis.ru

Ekaterina A. Kozlova – Boreskov Institute of Catalysis SB RAS, Lavrentieva Ave, 5, Novosibirsk, 630090, Russia; ORCID 0000-0001-8944-7666; kozlova@catalysis.ru

Conflict of interest: the authors declare no conflict of interest.